International Journal of Technology

Research Article

The Role of Graphene Oxide as a Filler and Lanthanum Nitrate as a Salt in Corn Starch-Based Solid Polymer Electrolytes

Rafi Athallah [1], Sylvia Ayu Pradanawati [2], Reffy Aldo Amanta [1], Azzah Dyah Pramata [3], Nezihe Ayas [4], Tetsuya Kida [5], Nur Laila Hamidah [1,*]

[1]Departement of Engineering Physics, Institut Teknologi Sepuluh Nopember, Kampus ITS Sukolilo, Surabaya 60111, Indonesia

[2]Department of Mechanical Engineering, Universitas Pertamina, Jalan Teuku Nyak Arief, Simprug Kebayoran Lama, Jakarta 12220, Indonesia

[3]Departement of Chemistry, Institut Teknologi Sepuluh Nopember, Kampus ITS Sukolilo, Surabaya 60111, Indonesia

[4]Eskisehir Technical University, Engineering Faculty, Department of Chemical Engineering, 2 Eylul Campus 26555, Eskisehir, Türkiye

[5]Division of Materials Science, Faculty of Advanced Science and Technology, Kumamoto University, Kumamoto 860-8555, Japan

[*]Corresponding author: nurlaila@its.ac.id; Tel.: (031) 594-7188

Abstract: Solid polymer electrolytes (SPE) with high ionic conductivity are in great demand for the effective application of solid-state electrochemical devices. Therefore, this study aimed to improve ionic conductivity of corn starch (CS)-based SPE by incorporating lanthanum nitrate salt and graphene oxide (GO) as filler. The solution casting method was used to produce a thin SPE film, and X-Ray Diffraction (XRD) investigations found that the SPE structure had a higher degree of amorphousness during the addition of salt and GO. Furthermore, the Fourier Transform Infrared (FTIR) Spectroscopy data presented a change in the functional group alongside an increased intensity in the C-O-H group, signifying the formation of hydrogen bonds with GO and the cleavage of the C-O-C chain due to the introduction of salt. The analysis conducted with the Scanning Electron Microscope (SEM) identified that the interaction with GO led to enhanced porosity, generating additional cavities in the SPE sample. The amorphous structure was confirmed through Differential Scanning Calorimetry (DSC), which showed a reduction in melting point with the incorporation of salt and GO. Increased ionic conductivity in SPE was observed in Electrochemical Impedance Spectroscopy (EIS) after GO incorporation. Ionic conductivity measured without the presence of filler was 9.95×10^{-7} S/cm while adding 1% of filler improved conductivity by 126.13% with a value of 2.25×10^{-6} S/cm. GO inclusion in CS-based SPE film enhanced the interaction between ions and polymer, promoting an increase in ionic conductivity. The results showed the possible applicability of electrochemical energy storage, such as lithium-ion batteries and supercapacitors.

Keywords: Graphene oxide; Ionic conductivity; Solid polymer electrolytes

1. Introduction

Energy is essential for human life because the majority of the income in poor households is used for energy needs. This commodity significantly affects the economic, social, and political fields (IEA, 2022). From the onset of the industrial revolution, fossil fuels have been used as an energy source (Wang and Azam, 2024; Setiawan and Asvial, 2016). However, fossils produce greenhouse gas (GHG) emissions that cause global warming (Whulanza et al., 2024). GHG emissions caused by fossil use increased significantly in 1950 and continued to rise until 2020 (UNEP, 2022; IPCC, 2015). In addressing these emissions, countries around the world are working to reduce the use of fossil fuels in accordance with the 2015 Paris Agreement, by transitioning to renewable energy (Aravindan et al., 2023; Kabeyi and Olanrewaju, 2022). The application of renewable energy technology requires electrochemical energy storage (EES) devices (Nugraha et al., 2023; AL Shaqsi et al., 2020). Therefore, the improvement of EES performance is needed to keep pace with the development of renewable energy technology in the future.

The performance of EES can be influenced by types of electrolytes, which often affect energy capacity, conductivity, cyclability, safety, and other properties (Xia et al., 2017). There are liquid and solid-state or solid polymer electrolytes (SPE) (Arrieta et al., 2022; Zhong et al., 2015). The liquid types are commonly used in commercialized EES, with advantages such as high conductivity and capacitance (Béguin et al., 2015). These have disadvantages, particularly in the field of safety due to flammability and poor thermal stability which are capable of intiating fire hazards (Sun et al., 2022; Jaumaux et al., 2021). The characteristics of SPE include low flammability, impressive flexibility, outstanding thermal stability, and high safety, but the possessed conductivity is lower (Yao et al., 2019).

Polyethylene (PE), polypropylene (PP), and polystyrene (PS) are examples of synthetic polymer majorly used in SPE because of the low cost, high strength, and durability (Saal et al., 2021). Synthetic polymer production causes environmental issues like pollution and GHG emissions (Atiwesh et al., 2021). This shows a need to conduct environmentally friendly fabrication of SPE with abundant materials and high conductivity. SPE can be alternatively produced using biopolymers obtained from biodegradable resources that are renewable, such as cellulose, pectin, gelatin, chitosan, and starch (Abdulwahid et al., 2023). Both cellulose and the derivatives are used as sustainable battery separators to reduce dependence on fossil resources because of the hydrophilicity, favorable mechanical and thermal characteristics, controllable porosity, and non-toxic material (Lizundia et al., 2020). Another material preferably used is starch which is easily obtained as well as composed of amylose and amylopectin. The amylose unit has a linear structure, while amylopectin is branched (Lai et al., 2022). Amylose composition easily interacts with salt than amylopectin, promoting the use of starch types consisting of high amylose levels as polymer host for the development of SPE (Lai et al., 2022). Corn starch (CS) is often selected due to the biodegradability, good solubility, low cost, easy availability, and renewability (Jiang et al., 2020). This comprises a higher amylose content compared to common starch products (Chauhan et al., 2020; Khiar and Arof, 2010), which leads to being used as polymer. Several studies conducted on CS-based SPE generated ionic conductivity value of 1.09×10^{-6} S/cm (Jothi et al., 2022).

A proportional increase in the amorphous property of SPE samples has been observed with rising ionic conductivity (Aziz and Abidin, 2015). Several previous investigations focused on adding salt as a dopant to improve SPE amorphousness. For example, a study combined SPE from polyvinyl alcohol (PVA) and polyvinylpyrrolidone (PVP) with sodium thiocyanate salt (NaSCN) to enhance amorphousness with conductivity of 8.1×10^{-5} S / cm (Badi et al., 2022). Other studies added salt to improve conductivity through the use of the rare earth element material. Rare earth element is known to have a better performance than alkali metals because of the intercalations of cations, specifically La^{3+}, into GO membranes which significantly improve proton conductivity at 60°C and higher temperatures (Hamidah et al., 2019). Ali and Maiz (2018) used lanthanum nitrate as a dopant in PVA to enhance the amorphous nature of polymer with salt addition. Lanthanum nitrate has a

higher solubility compared to other types of lanthanum salt, and the good solubility facilitates easier SPE synthesis (Wijanarko et al., 2024). This is a promising dopant salt because of the good solubility, the potential to make polymer more amorphous, and the interaction with GO, which all increase conductivity in SPE.

GO is a material with electrolyte potential due to being rich in oxygen functional groups as a medium for ionic movement to produce high conductivity (Ogata et al., 2017; Hatakeyama et al., 2015). The oxygen groups enable interaction with other materials through the process of hydrogen bonding, as well as ionic and electrostatic interactions (Liu et al., 2019). Some studies were conducted on SPE using various GO concentrations in several polymer bases. For example, Wen et al. (2021a) obtained ionic conductivity value of 1.54×10^{-5} S/cm at room temperature with a concentration of 1wt% of GO used as filler in PE oxide-based polymer electrolytes (Wen et al., 2021a). Another study by Jia et al. (2018) produced ionic conductivity value of 4.03×10^{-4} S/cm with 1wt% of GO in polyacrylonitrile-based SPE at room temperature (Jia et al., 2018). In addition, Electrochemical Impedance Spectroscopy (EIS) characterization was performed across a wide range of temperature variations. The results showed that GO had good thermal stability at high temperatures, significantly increased conductivity with a small 1wt.% concentration, and maintained the conductivity value till 100°C with the presence of lanthanum nitrate (Kumar and Srivastava, 2021; Hamidah et al., 2019). The ease of interacting with other materials facilitates the reaction between GO and starch to form hydrogen bonding in the OH functional group (Rapisarda et al., 2021; Li et al., 2011). Investigations using rare earth elements as salt in this context are limited, and the combined application of GO and CS has not been reported. Therefore, this study aimed to improve ionic conductivity using GO as filler in SPE based on CS and lanthanum nitrate. Ionic conductivity is essential for the performance of EES systems, such as lithium-ion batteries and supercapacitors (Awang et al., 2022).

2. Methods

2.1. GO synthesis

GO was synthesized through the modified Tour Method using expanded graphite, as documented in a prior study (Hamidah et al., 2020). Expanded graphite was sourced from Ito Graphite Co., Ltd., Japan. Initially, 3.0 g of expanded graphite with a median diameter of 5-50 μm was thoroughly combined with 18 g of potassium permanganate which was purchased from Sigma-Aldrich. Subsequently, 360 mL of a concentrated H_2SO_4/H_3PO_4 solution was introduced, and the resulting mixture was subjected to be stirred and heated to 50 °C for 12 hours in an oil bath. When room temperature was attained, the mixture was combined with ice, and 6 mL of H_2O_2 was introduced. The solid was centrifuged at 4000 rpm, washed with 5% HCl and water for 10 minutes on three occasions, dispersed in water, sonicated for 5 hours, and spun again at 10000 rpm to obtain exfoliated solids.

2.2. CS-based SPE fabrication

CS-based SPE in this study was synthesized using the solution casting method (Awang et al., 2022). CS was freely purchased under the brand Maizenaku (Indonesian brand) with starch content of 75%, and Glycerol 98%, while lanthanum nitrate $La(NO_3)_3$ 99.9% was purchased from Sigma-Aldrich. SPE synthesis was carried out with five variations, starting from CS and salt only, followed by using CS at concentrations of 0.5wt%, 1wt%, 1.5wt%, and 2wt% as host polymers, incorporated with salt and GO. The details regarding the composition are presented in Table 1. SPE synthesis was initiated by sonicating GO in aquades first for 1 hour. Subsequently, lanthanum nitrate, glycerol, and CS were dissolved in GO solution with a magnetic stirrer for 15 minutes. The mixture was transferred into a water bath and a magnetic stirrer was used to stir it at 80°C for 1 hour with a speed of 200 RPM until a homogeneous state was obtained. This was cooled, bubbles were removed, and the the mixture was poured into a petri dish, then dried for 12 hours at 50°C in a B-One Type: OV-30 Digital Oven until a thin SPE film formed visibly.

Table 1 The composition of synthesized membrane

Symbol	Aquades	Corn Starch	*Lanthanum nitrate*	Glycerol	*Graphene oxide (wt %)*
CSLa					0% (0 g)
CSLa:GO 0.5%					0.5% (0.1 g)
CSLa:GO 1%	20 ml	2 g	0.5 g	0.7 ml	1% (0.2 g)
CSLa:GO 1.5%					1.5% (0.3 g)
CSLa:GO 2%					2% (0.4 g)

2.3. SPE characterization

The SPE samples underwent various tests like X-ray diffraction (XRD), Fourier Transform Infrared (FTIR) Spectroscopy, Scanning Electron Microscope (SEM), Differential Scanning Calorimetry (DSC), and EIS. The PanAnalytical XRD E'xpert PRO was used to determine the amorphous or crystalline structure of the SPE film. XRD measurements used CuKα wavelengths of 1.54056 Å, as well as Ni filters at 40 kV and 100 mA. The analysis of samples was performed in the range of 2θ = 5-50°, with a scanning speed of 0.5°C/min and 0.05°/step at room temperature. Meanwhile, the FTIR characterization was conducted using the Thermo Scientific Nicolet iS10 type. This test aimed to identify the interactions between functional groups of CS, $La(NO_3)_3$, and GO. The SEM characterization was performed with the FEI Inspect S50 model which was used to analyze the surface morphology of samples at magnifications of 1000x and 10,000x. Additionally, Mettler Toledo equipment with a scan rate of 10 °C per minute, covering temperatures from 25 to 160°C, was used to assess the thermal stability of samples. The EIS test was conducted using the Corrtest type CS Series Electrochemical Workstation equipment to carried out AC impedance spectroscopy across a frequency ranging from 1 MHz - 1 Hz and a signal of 10 mV.

3. Results and Discussion

3.1. Synthesis results

The synthesis of SPE based on CS used lanthanum nitrate salt and GO filler added at different amounts, including 0wt%, 0.5wt%, 1wt%, 1.5wt%, and 2wt% as shown in Figure 1. The results in the form of thin films changed from clear to dark brown as more GO was added becuase GO could absorb ultraviolet and visible light (Tene et al., 2023; Chen et al., 2021). The change in color showed that GO dispersed evenly across the SPE films (Hu et al., 2020).
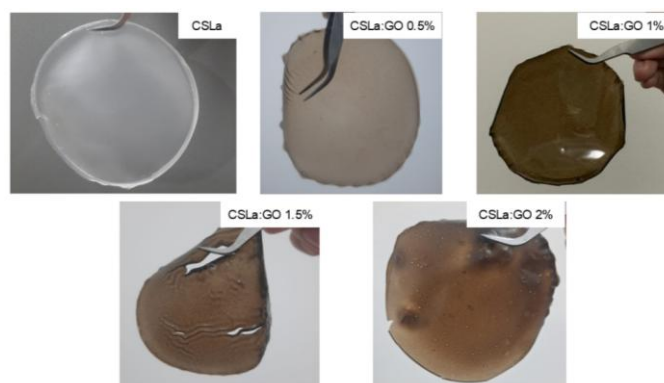

Figure 1 Synthesis results of SPE membrane with an increasing amount of GO

3.2. XRD results

XRD graphs can be used in identifying the amorphous and crystallinity structure of SPE samples. The patterns generated on these graphs prior to and after incorporating GO were compared to particularly determine how the applied filler affected crystallinity. Moreover, the comparison was

conducted by monitoring the intensity at specific diffraction angles, and the test results were presented as shown in Figure 2.
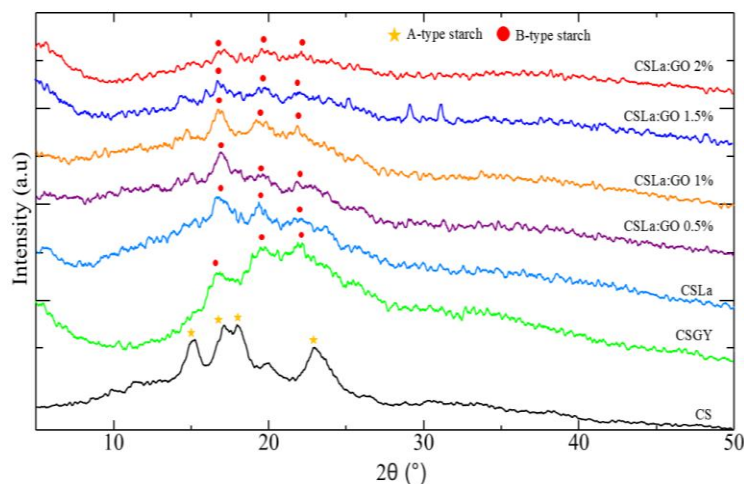

Figure 2 XRD patterns of CS-based SPE incorporated with lanthanum nitrate salt and GO filler

The fundamental material used to manufacture SPE samples with characteristics that have peaks at angles of 15°, 17°, 17.5°, and 23° is type A CS shown in Figure 2. The structure of CS transforms from type A to B after gelatinization, as signified by the peaks of the angles in starch post incorporation of glycerol or salt at 17°, 19.5°, and 22° (Kong et al., 2014). From the observation, a more open polymorph structure comprising a hydrated helical core is found in type B (Xu et al., 2024). The transformation process is followed by decreased crystallinity and increased levels of amylose because of the ratio between water molecules and helical structures present in type B starch that has bigger sizes (Qiao et al., 2017; Tester et al., 2004). The results of characterization showed that the XRD analysis, following the addition of salt and GO, caused polymer to become more amorphous. An amorphous polymer is more loosely arranged compared to a crystalline structure, facilitating easier ion transfer. Figure 2 did not show the high peak of GO which was around an angle of 10°, and the crystalline peaks in starch appeared to decrease in intensity after adding salt along with 0.5%, 1%, 1.5%, and 2% GO.

Table 2 Calculation results of d-spacing (d) and strain (ε)

Sample	Peak 1		Peak 2		Peak 3		Average	
	d	E	d	E	d	E	d	E
CSLa	5.225	1.803	4.593	1.676	4.000	1.560	4.606	1.680
CSLa:GO 0.5%	5.262	1.821	4.575	3.527	4.014	1.712	4.617	2.353
CSLa:GO 1%	5.277	1.824	4.615	3.529	4.057	1.816	4.650	2.390
CSLa:GO 1.5%	5.209	2.720	4.492	3.495	3.987	1.886	4.563	2.701
CSLa:GO 2%	5.212	2.773	4.470	3.785	4.003	2.367	4.562	2.975

The values of d-spacing (d) and strain (ε) calculated are presented in Table 2. The results of d-spacing showed that GO addition increased until the concentration reached 1%, and d-spacing decreased when the concentration was exceeded. Increasing the values of d-spacing represents an expansion in free space between segments of polymer to facilitate easy ion transport (Tian et al., 2022). Moreover, a decrease in the values of d-spacing after adding GO by more than 1% suggests a reduction in free space for the movement of ions because of the possibility that a large GO concentration can close the space (Islam and Mollik, 2020). There is an occurrence of XRD peak widening due to strains, in which the high values signify increased sample flexibility. GO addition enhances sample flexibility with a wider distance between segments allowing easier movement to increase ion conductivity (Fan et al., 2019; Nasiri-Tabrizi, 2014).

3.3. Fourier transform infrared (FTIR) spectroscopy results

FTIR spectroscopy is used to identify the effect of salt and GO filler addition on the functional groups of synthesized SPE samples. The FTIR characterization results obtained from SPE samples are shown in Figure 3A.
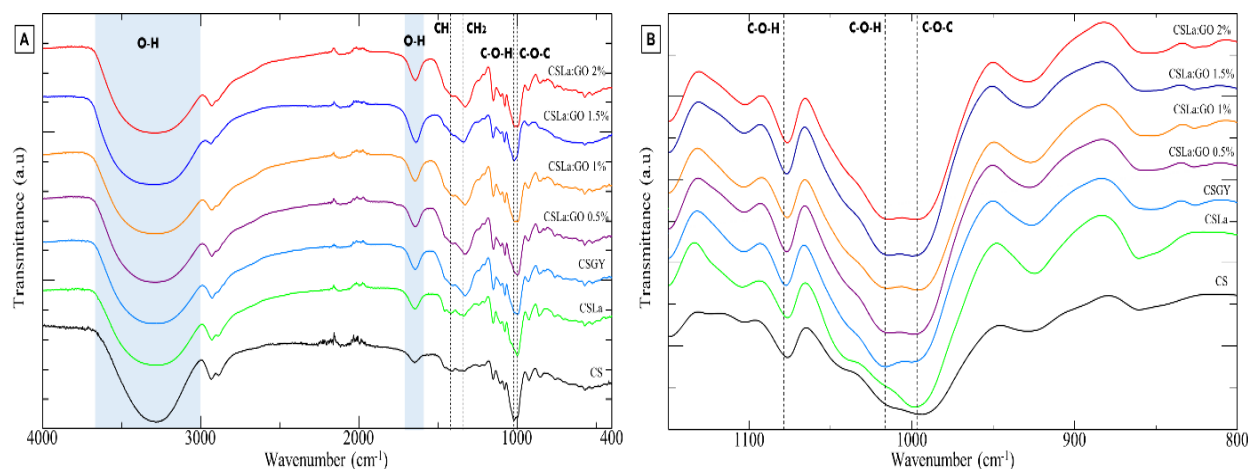

Figure 3 (A) FTIR spectra of CS-based SPE with the addition of lanthanum nitrate as salt and GO as filler; (B) The magnification of FTIR spectra in wavenumber range of 1050 – 1200 cm^{-1}

FTIR characterization results showed that peaks around the area 3300 – 3400 cm^{-1} were O-H group stretching. Furthermore, 2927 cm^{-1}, 1650 cm^{-1}, 1300 – 1500 cm^{-1}, 1151 cm^{-1} and 1077 cm-1, 1020 cm^{-1}, and 997 cm^{-1}, represented C-H group stretching vibration, O-H group bending, CH and CH$_2$ deformation in CH$_2$OH, C-O stretching vibration in C-O-H, C-O-H deformation, and C-O \ stretching vibration in C-O-C, respectively (Islam and Mollik, 2020; Ismail and Zaaba, 2012; Li et al., 2011). The results showed the termination of the C-O-C chain in CS because of salt addition and the formation of hydrogen bonds between CS and GO. This interaction led to an increase in the amorphous nature of polymer, as the interactions between hydrogen bonds generated shorter amylose chains. Consequently, the C-O-C chain termination produced a looser spatial arrangement. Figure 3B shows changes around 997 – 1020 cm^{-1}, specifically salt addition increases the intensity in the 1020 cm^{-} area and decreases the intensity in the 997 cm^{-1} area. This may suggest the occurrence of ring opening in the C-O-C functional group which forms C-O-H due to the addition of lanthanum nitrate salt. La^{3+} from lanthanum allows Lewis acid interaction with oxygen in C-O-C, enabling H$_2$O as a nucleophile to attack one of the carbons and break the bond into C-O. The C-O bond can interact with hydrogen from H$_2$O to form C-O-H (Makrygenni et al., 2019). Moreover, salt addition increased the intensity in the 1327 cm^{-1} area, signifying that La^{3+} reacted with the OH functional group in CH$_2$OH through electrostatic interaction.

Figure 3B shows that peak shift occurs after GO addition in the areas of 1151 cm^{-1} and 1077 cm^{-1} to attain lower values. Changes found in 1200 – 900 cm^{-1} post GO addition represent hydrogen bonding between GO and CS. The hydrogen in the C-O-H functional group of starch can interact with oxygen component of the hydroxyl group (OH) in GO to produce a hydrogen bond because the oxygen atom has a high electronegativity (Azli et al., 2017; Li et al., 2011).

3.4. Scanning electron microscopy (SEM) results

SEM is used to analyze the surface morphology and microstructural changes in CSLa and CSLa-GO samples. Based on the SEM images in Figure 4, the surface morphology and porosity of CSLa and CSLa-GO samples change with increasing GO concentration. From the images, CSLa used as the base sample is found to have a relatively smooth surface with a low void formation area, which reflects a dense and uniform material structure (Wen et al., 2021b). However, GO addition leads to a progressive increase in the distribution surface irregularities and voids, where the CSLa:GO 2% sample has the most pronounced roughness (Bashirpour-bonab, 2022; Elerian et al., 2022). This

structural modification shows how GO disperses across polymer matrix, disrupting the surface uniformity and enhancing the development of void networks (Bashirpour-bonab, 2022).

The CSLa-GO samples had more pores. correlating with the greater state of surface roughness. Materials with numerous void distributions tend to have this feature (Awang et al., 2021). The porosity ranged from 0.1923% in CSLa to 1.5349% in CSLa:GO 2% and the observed increase represented significant changes in surface morphology, showing how polymer matrix and GO interacted (Huy et al., 2021; Sabrina et al., 2019).
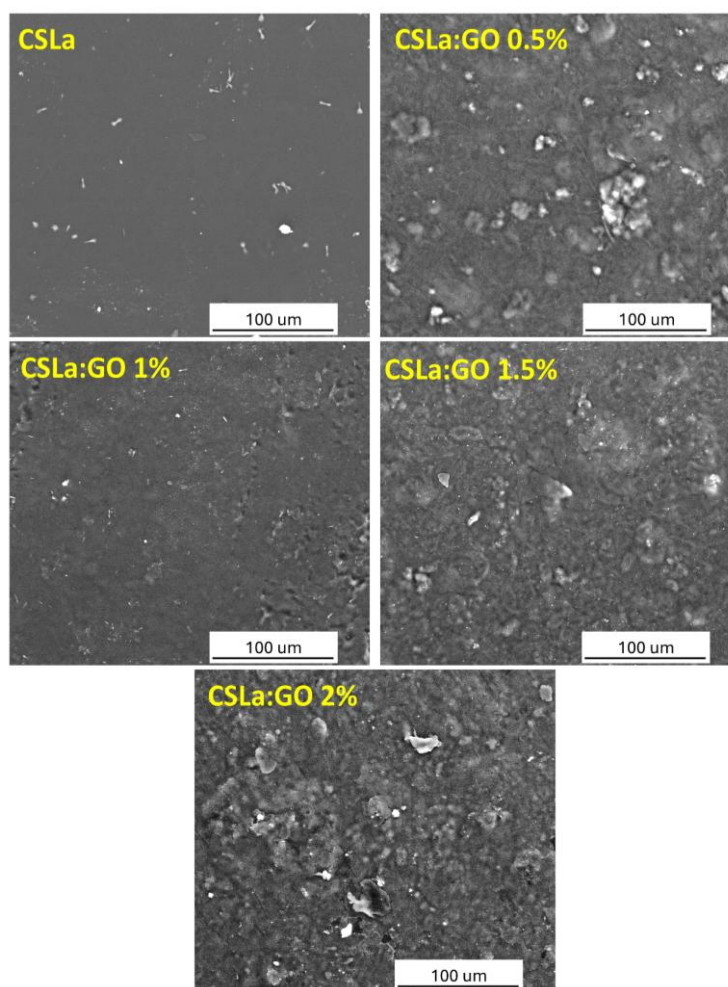

Figure 4 SEM images of SPE with 1000x magnification

3.5. Differential scanning calorimetry (DSC) results

DSC characterization is used for thermal analysis in SPE samples. The results of DSC characterization are shown in Figure 5 in the form of endothermic peaks. DSC results showed that salt addition to SPE led to a decrease in the melting point (T_m) of samples as signified by a shift from a higher to lower temperature compared to pure CS. Additionally, GO incorporation as filler shifted the melting point to a lower temperature compared to pure CS or salt-added samples. The melting point of CS, CSLa, and CSLa:GO 2% samples was ~81°C, ~72°C, and ~68°C, respectively. The melting point shift to a lower temperature suggested that the samples became more amorphous, facilitating an increase in ionic conductivity (Ni'mah et al., 2021).
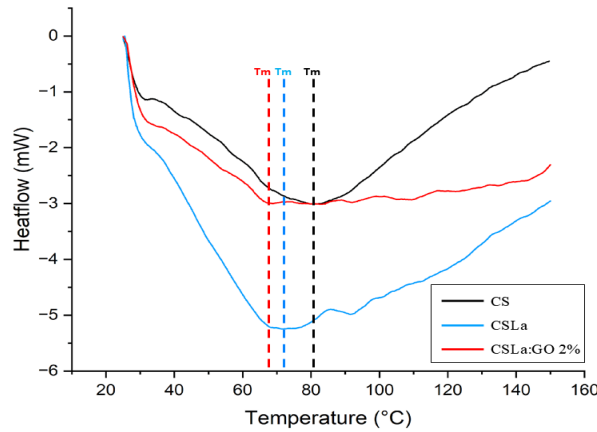
Figure 5 DSC thermogram of CS-based SPE with the addition of lanthanum nitrate as salt and GO as filler

3.6. EIS results

EIS testing is specifically targete at calculating ionic conductivity value of SPE samples. The results are expressed as data presented in a Nyquist graph form, with y-axis being $Z_{imaginer}$ (Ω) and x-axis being Z_{real} (Ω). A Nyquist graph shows the electrochemical behavior of a system, with each data point representing the SPE impedance measured at a specific frequency. In the range of high-to-low frequency, the graph forms a semicircle, which the bulk resistance (Rb) value intersects between the depressed semicircle at low frequency and the x-axis (Abdul Halim et al., 2021). The measurement results fit to the equivalent circuit that describes the system as shown in Figure 6. Moreover, ionic conductivity of SPE membrane is calculated using equation 1.
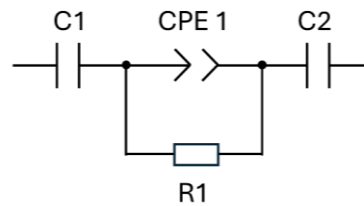

Figure 6 Equivalent circuit for SPE

$$\sigma = \frac{l}{Rb \times A} \tag{1}$$

where σ is ionic conductivity of SPE, l represents the SPE thickness, Rb is SPE bulk resistance, and A denotes SPE surface area.

The equivalent circuit describes SPE as a dielectric material squeezed by two blocking electrodes, namely C1 and C2, according to measurements where SPE is squeezed between two stainless steels. This is composed of the capacitance of the constant phase element (CPE) and resistance (R1) as bulk resistance (Rb) arranged in parallel to describe SPE as a dielectric material. The use of CPE in the equivalent series is suitable to describe a non-ideal system. The fitting in this study was conducted based on Figure 6 to determine Rb value for the calculation of ionic conductivity through equation (1). The obatined results of the EIS test are presented in Figure 7.

Table 3 shows the highest ionic conductivity of CS-based SPE and lanthanum nitrate samples comprising GO filler with a concentration of 1% which has a value of $\sigma = 2.25 \times 10^{-6}$ S/cm. SPE with GO incorporated at a concentration greater than 1% has decreased conductivity, signifying that the addition of 1% filler is the optimum value. There is a decrease in ionic conductivity after the addition of GO exceeds the concentration of 1%. This occurs because of a potential blocking effect where polymer chain movement is reduced due to close or decreasing distance between fillers (Dissanayake et al., 2003).
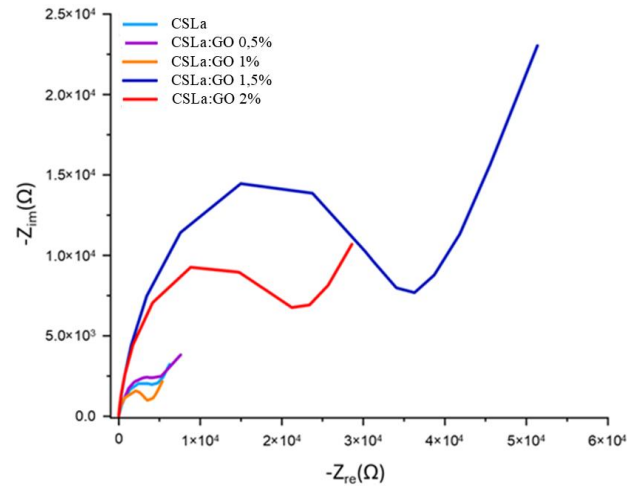
Figure 7 Nyquist plot of CS-based SPE with the addition of lanthanum nitrate as salt and GO as filler

Table 3 Ionic conductivity calculation results

Sample	l (cm)	A (cm²)	Rb (ohm)	σ (S/cm)
CSGY	0.030	3.14	28500	3.39×10^{-7}
CSLa	0.018	3.14	6000	9.95×10^{-7}
CSLa:GO 0.5%	0.024	3.14	6250	1.12×10^{-6}
CSLa:GO 1%	0.026	3.14	3680	2.25×10^{-6}
CSLa:GO 1.5%	0.029	3.14	36300	2.54×10^{-7}
CSLa:GO 2%	0.024	3.14	22330	3.42×10^{-7}

The value of ionic conductivity is determined by the ease of ion mobility. Therefore, ions in SPE need to move through polymer chains, a process known as segmental motion. Figure 8 shows the motion where ions are hopping from one segment to another in polymer chains. The more amorphous structure of the looser SPE permits extended distances that enable ions to travel more easily, compared to crystalline structures, resulting in enhanced ionic conductivity.
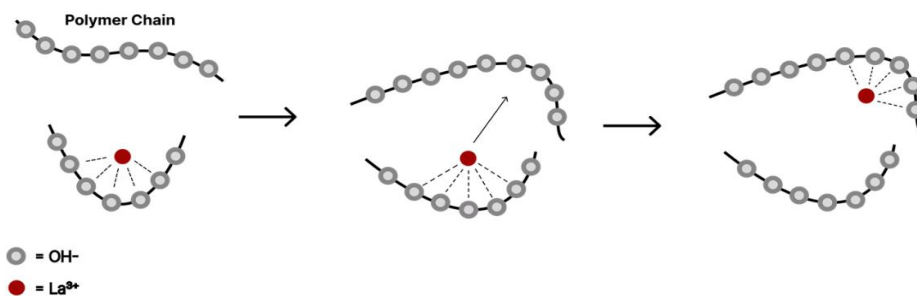

Figure 8 Segmental motion mechanism of CS-based SPE

4. Conclusions

In conclusion, this study found that incorporating GO filler during the conducted characterization process caused the SPE samples to become more amorphous, as evidenced by a decrease in crystallinity from the XRD results. The increasingly amorphous samples occurred due to salt interactions cleaving C-O-C into C-O-H and GO hydrogen bonding with CS based on changes in FTIR. SEM testing showed morphological changes after GO addition to become more porous. The amorphous results were strengthened by the DSC test which lowered the melting point post GO addition. Therefore, increasingly amorphous samples allowed a rise in ionic conductivity. The

maximum conductivity value of 2.25×10^{-6} S/cm was achieved with the incorporation of GO filler at a concentration of 1%. Increasing the concentration of GO beyond 1% intiated a reduction of ionic conductivity due to a blocking effect.

Acknowledgements

Author Contributions

Experimental, data curation, formal analysis, visualization and writing-original draft, R.A.; Experimental, Data curation, Formal analysis, Visualization, R.A.A.; investigation, supervision, S.A.P.; formal analysis, investigation, A.D.P. and N.A.; conceptualization, supervision, T.K.; Conceptualization, data curation, visualization, supervision, and writing-review & editing, N.L.H.

Conflict of Interest

The authors declare no conflicts of interest.

References

Abdul Halim, SI, Chan, CH & Apotheker, J 2021, 'Basics of teaching electrochemical impedance spectroscopy of electrolytes for ion-rechargeable batteries – part 1: a good practice on estimation of bulk resistance of solid polymer electrolytes', *Chemistry Teacher International*, vol. 3, pp. 105–115, https://doi.org/10.1515/cti-2020-0011

Abdulwahid, RT, Aziz, SB & Kadir, MFZ 2023, 'Replacing synthetic polymer electrolytes in energy storage with flexible biodegradable alternatives: sustainable green biopolymer blend electrolyte for supercapacitor device', *Materials Today Sustainability*, vol. 23, p. 100472, https://doi.org/10.1016/j.mtsust.2023.100472

AL Shaqsi, AZ, Sopian, K & Al-Hinai, A 2020, 'Review of energy storage services, applications, limitations, and benefits', *Energy Reports*, vol. 6, pp. 288–306, https://doi.org/10.1016/j.egyr.2020.07.028

Ali, FM & Maiz, F 2018, 'Structural, optical and AFM characterization of PVA:La3+ polymer films', *Physica B: Condensed Matter*, vol. 530, pp. 19–23, https://doi.org/10.1016/j.physb.2017.10.124

Aravindan, KL, Izzat, MA, Ramayah, T, Chen, TS, Choong, YV, Annamalah, S, Ilhavenil, N & Ahmad, AB 2023, 'Determinants of electric car patronage intention', *International Journal of Technology*, vol. 14, pp. 291–319, https://doi.org/10.14716/ijtech.v14i6.6624

Arrieta, A, Barrera, I & Mendoza, J 2022, 'Impedantiometric behavior of solid biopolymer electrolyte elaborated from cassava starch synthesized in different pH', *International Journal of Technology*, vol. 13, pp. 291–319, https://doi.org/10.14716/ijtech.v13i4.5612

Atiwesh, G, Mikhael, A, Parrish, CC, Banoub, J & Le, T-AT 2021, 'Environmental impact of bioplastic use: a review', *Heliyon*, vol. 7, no. 9, article e07918, https://doi.org/10.1016/j.heliyon.2021.e07918

Awang, FF, Hassan, MF & Kamarudin, KH 2021, 'Corn starch doped with sodium iodate as solid polymer electrolytes for energy storage applications', *Acta Polytechnica*, vol. 61, pp. 497–503, https://doi.org/10.14311/AP.2021.61.0497

Awang, FF, Hassan, MF & Kamarudin, KH 2022, 'Study on ionic conductivity, dielectric and electrochemical properties of solid polymer electrolyte for battery applications', *Ionics*, vol. 28, pp. 1249–1263, https://doi.org/10.1007/s11581-022-04444-3

Aziz, SB & Abidin, ZHZ 2015, 'Ion-transport study in nanocomposite solid polymer electrolytes based on chitosan: electrical and dielectric analysis', *Journal of Applied Polymer Science*, vol. 132, no. 15, https://doi.org/10.1002/app.41774

Azli, AA, Manan, NSA & Kadir, MFZ 2017, 'The development of Li+ conducting polymer electrolyte based on potato starch/graphene oxide blend', *Ionics*, vol. 23, pp. 411–425, https://doi.org/10.1007/s11581-016-1874-z

Badi, N, Theodore, AM, Alghamdi, SA, Al-Aoh, HA, Lakhouit, A, Roy, AS, Alatawi, AS & Ignatiev, A 2022, 'Fabrication and characterization of flexible solid polymers electrolytes for supercapacitor application', *Polymers*, vol. 14, no. 18, article 3837, https://doi.org/10.3390/polym14183837

Bashirpour-Bonab, H 2022, 'Analysis of the effect of graphene oxide on polymer electrolytes based on PVDF for lithium-ion battery', *International Journal of Energy Research*, vol. 46, https://doi.org/10.1002/er.8278

Béguin, F, Presser, V, Balducci, A & Frackowiak, E 2015, 'Carbons and electrolytes for advanced supercapacitors', *Advanced Materials*, vol. 26, pp. 2219–2251, https://doi.org/10.1002/adma.201304137

Chauhan, JK, Yadav, D, Yadav, M, Kumar, M, Tiwari, T & Srivastava, N 2020, 'NaClO4 added, corn and arrowroot starch based economical, high conducting electrolyte membranes for flexible energy devices', *SN Applied Sciences*, vol. 2, pp. 1–12, https://doi.org/10.1007/s42452-020-2660-0

Chen, J, Perez-Page, M, Ji, Z, Zhang, Z, Guo, Z & Holmes, S 2021, 'One-step electrochemical exfoliation of natural graphite flakes into graphene oxide for polybenzimidazole composite membranes giving enhanced performance in high temperature fuel cells', *Journal of Power Sources*, vol. 491, article 229550, https://doi.org/10.1016/j.jpowsour.2021.229550

Dissanayake, MAKL, Jayathilaka, PARD, Bokalawala, RSP, Albinsson, I & Mellander, B-E 2003, 'Effect of concentration and grain size of alumina filler on the ionic conductivity enhancement of the (PEO)9LiCF3SO3:Al2O3 composite polymer electrolyte', *Journal of Power Sources*, vol. 119–121, pp. 409–414, https://doi.org/10.1016/S0378-7753(03)00262-3

Elerian, AF, Abu-Saied, MA, Abd-Elnaim, GH & Elnaggar, EM 2022, 'Development of polymer electrolyte membrane based on poly(vinyl chloride)/graphene oxide modified with zirconium phosphate for fuel cell applications', *Journal of Polymer Research*, vol. 30, article 6, https://doi.org/10.1007/s10965-022-03317-7

Fan, X, Nie, W, Tsai, H, Wang, N, Huang, H, Cheng, Y, Wen, R, Ma, L, Yan, F & Xia, Y 2019, 'PEDOT:PS S for flexible and stretchable electronics: modifications, strategies, and applications', *Advanced Science*, vol. 6, article 1900813, https://doi.org/10.1002/advs.201900813

Hamidah, NL, Shintani, M, Ahmad Fauzi, AS, Mission, EG, Hatakeyama, K, Quitain, AT & Kida, T 2019, 'Improving the proton conductivity of graphene oxide membranes by intercalating cations', *SN Applied Sciences*, vol. 1, pp. 1–8

Hamidah, NL, Shintani, M, Ahmad Fauzi, AS, Putri, GK, Kitamura, S, Hatakeyama, K, Sasaki, M, Quitain, AT & Kida, T 2020, 'Graphene oxide membranes with cerium-enhanced proton conductivity for water vapor electrolysis', *ACS Applied Nano Materials*, vol. 3, pp. 4292–4304, https://doi.org/10.1021/acsanm.0c00439

Hatakeyama, K, Islam, MS, Michio, K, Ogata, C, Taniguchi, T, Funatsu, A, Kida, T, Hayami, S & Matsumoto, Y 2015, 'Super proton/electron mixed conduction in graphene oxide hybrids by intercalating sulfate ions', *Journal of Materials Chemistry A*, vol. 3, pp. 20892–20895, https://doi.org/10.1039/C5TA05653E

Hu, Z, Zhang, X & Chen, S 2020, 'A graphene oxide and ionic liquid assisted anion-immobilized polymer electrolyte with high ionic conductivity for dendrite-free lithium metal batteries', *Journal of Power Sources*, vol. 477, article 228754, https://doi.org/10.1016/j.jpowsour.2020.228754

Huy, VPH, So, S & Hur, J 2021, 'Inorganic fillers in composite gel polymer electrolytes for high-performance lithium and non-lithium polymer batteries', *Nanomaterials*, vol. 11, no. 3, article 614, https://doi.org/10.3390/nano11030614

IEA 2022, *International Energy Agency (IEA) World Energy Outlook 2022*, viewed 15 March 2025, (https://www.iea.org/reports/world-energy-outlook-2022/executive-summary)

IPCC 2015, *AR5 Synthesis Report: Climate Change 2014*, IPCC, viewed 15 March 2025, (https://www.ipcc.ch/report/ar5/syr/)

Islam, MR & Mollik, SI 2020, 'Enhanced electrochemical performance of flexible and eco-friendly starch/graphene oxide nanocomposite', *Heliyon*, vol. 6, article e05292, https://doi.org/10.1016/j.heliyon.2020.e05292

Ismail, H & Zaaba, NF 2012, 'The mechanical properties, water resistance and degradation behaviour of silica-filled sago starch/PVA plastic films', *Journal of Elastomers & Plastics*, vol. 46, pp. 96–109, https://doi.org/10.1177/0095244312462163

Jaumaux, P, Wu, J, Shanmukaraj, D, Wang, Y, Zhou, D, Sun, B, Kang, F, Li, B, Armand, M & Wang, G 2021, 'Non-flammable liquid and quasi-solid electrolytes toward highly-safe alkali metal-based batteries', *Advanced Functional Materials*, vol. 31, article 2008644, https://doi.org/10.1002/adfm.202008644

Jia, W, Li, Z, Wu, Z, Wang, L, Wu, B, Wang, Y, Cao, Y & Li, J 2018, 'Graphene oxide as a filler to improve the performance of PAN-LiClO4 flexible solid polymer electrolyte', *Solid State Ionics*, vol. 315, pp. 7–13, https://doi.org/10.1016/j.ssi.2017.11.026

Jiang, T, Duan, Q, Zhu, J, Liu, H & Yu, L 2020, 'Starch-based biodegradable materials: challenges and opportunities', *Advanced Industrial and Engineering Polymer Research*, vol. 3, pp. 8–18, https://doi.org/10.1016/j.aiepr.2019.11.003

Jothi, MA, Vanitha, D & Sundaramahalingam, K 2022, 'Utilisation of corn starch in production of eco-friendly polymer electrolytes for proton battery applications', *International Journal of Hydrogen Energy*, vol. 47, pp. 28763–28772, https://doi.org/10.1016/j.ijhydene.2022.06.192

Kabeyi, MJB & Olanrewaju, OA 2022, 'Sustainable energy transition for renewable and low carbon grid electricity generation and supply', *Frontiers in Energy Research*, vol. 9, pp. 1–45, https://doi.org/10.3389/fenrg.2021.743114

Khiar, ASA & Arof, AK 2010, 'Conductivity studies of starch-based polymer electrolytes', *Ionics*, vol. 16, pp. 123–129, https://doi.org/10.1007/s11581-009-0356-y

Kong, L, Lee, C, Kim, SH & Ziegler, GR 2014, 'Characterization of starch polymorphic structures using vibrational sum frequency generation spectroscopy', *The Journal of Physical Chemistry B*, vol. 118, pp. 1775–1783, https://doi.org/10.1021/jp411130n

Kumar, N & Srivastava, VC 2021, 'La2O3 nanorods - reduced graphene oxide composite as a novel catalyst for dimethyl carbonate production via transesterification route', *Materials Today Communications*, vol. 29, article 102974, https://doi.org/10.1016/j.mtcomm.2021.102974

Lai, DS, Osman, AF, Adnan, SA, Ibrahim, I, Salimi, MNA & Alrashdi, AA 2022, 'Effective aging inhibition of the thermoplastic corn starch films through the use of green hybrid filler', *Polymers*, vol. 14, no. 13, article 2567, https://doi.org/10.3390/polym14132567

Li, R, Liu, C & Ma, J 2011, 'Studies on the properties of graphene oxide-reinforced starch biocomposites', *Carbohydrate Polymers*, vol. 84, pp. 631–637, https://doi.org/10.1016/j.carbpol.2010.12.041

Liu, Z, Rios-Carvajal, T, Andersson, MP, Ceccato, M, Stipp, SLS & Hassenkam, T 2019, 'Ion effects on molecular interaction between graphene oxide and organic molecules', *Environmental Science: Nano*, vol. 6, pp. 2281–2291, https://doi.org/10.1039/c9en00274j

Lizundia, E, Costa, CM, Alves, R & Lanceros-Méndez, S 2020, 'Cellulose and its derivatives for lithium ion battery separators: a review on the processing methods and properties', *Carbohydrate Polymer Technologies and Applications*, vol. 1, article 100001, https://doi.org/10.1016/j.carpta.2020.100001

Makrygenni, O, Bentaleb, FL, Brouri, D, Proust, A, Launay, F & Villanneau, R 2019, 'Selective uptake of La3+ ions with polyoxometalates-functionalized mesoporous SBA-15: an EXAFS study', *Microporous and Mesoporous Materials*, vol. 287, pp. 264–270, https://doi.org/10.1016/j.micromeso.2019.06.004

Nasiri-Tabrizi, B 2014, 'Thermal treatment effect on structural features of mechano-synthesized fluorapatite-titania nanocomposite: a comparative study', *Journal of Advanced Ceramics*, vol. 3, pp. 31–42, https://doi.org/10.1007/s40145-014-0090-4

Ni'mah, YL, Muhaiminah, ZH & Suprapto, S 2021, 'Increase of solid polymer electrolyte ionic conductivity using nano-SiO$_2$ synthesized from sugarcane bagasse as filler', *Polymers*, vol. 13, no. 23, article 4240, https://doi.org/10.3390/polym13234240

Nugraha, AF, Ratri, CR, Arundati, AH, Aguta, TB, Rohib, R, Chalid, M & Astutiningsih, S 2023, 'Effect of coagulation bath composition on cellulose-based polymer electrolyte fabricated via non-solvent-induced phase separation method', *International Journal of Technology*, vol. 14, pp. 291–319, https://doi.org/10.14716/ijtech.v14i7.6677

Ogata, C, Kurogi, R, Awaya, K, Hatakeyama, K, Taniguchi, T, Koinuma, M & Matsumoto, Y 2017, 'All-graphene oxide flexible solid-state supercapacitors with enhanced electrochemical performance', *ACS Applied Materials & Interfaces*, vol. 9, pp. 26151–26160, https://doi.org/10.1021/acsami.7b04180

Qiao, D, Zhang, B, Huang, J, Xie, F, Wang, DK, Jiang, F, Zhao, S & Zhu, J 2017, 'Hydration-induced crystalline transformation of starch polymer under ambient conditions', *International Journal of Biological Macromolecules*, vol. 103, pp. 152–157, https://doi.org/10.1016/j.ijbiomac.2017.05.008

Rapisarda, M, Marken, F & Meo, M 2021, 'Graphene oxide and starch gel as a hybrid binder for environmentally friendly high-performance supercapacitors', *Communications Chemistry*, vol. 4, article 169, https://doi.org/10.1038/s42004-021-00604-0

Saal, A, Hagemann, T & Schubert, US 2021, 'Polymers for battery applications—active materials, membranes, and binders', *Advanced Energy Materials*, vol. 11, article 2001984, https://doi.org/10.1002/aenm.202001984

Sabrina, Q, Sohib, A & Lestariningsih, T 2019, 'The effect of (TiO2 and SiO2) nano-filler on solid polymer electrolyte based LiBOB', *Journal of Physics: Conference Series*, vol. 1191, no. 1, article 012028, https://doi.org/10.1088/1742-6596/1191/1/012028

Setiawan, EA & Asvial, M 2016, 'Renewable energy's role in a changing world', *International Journal of Technology*, vol. 7, pp. 291–319, https://doi.org/10.14716/ijtech.v7i8.7216

Sun, CC, You, AH & Teo, LL 2022, 'XRD measurement for particle size analysis of PMMA polymer electrolytes with SiO2', *International Journal of Technology*, vol. 13, pp. 291–319, https://doi.org/10.14716/ijtech.v13i6.5927

Tene, T, Guevara, M, Benalcázar Palacios, F, Morocho Barrionuevo, TP, Vacacela Gomez, C & Bellucci, S 2023, 'Optical properties of graphene oxide', *Frontiers in Chemistry*, vol. 11, https://doi.org/10.3389/fchem.2023.1214072

Tester, RF, Karkalas, J & Qi, X 2004, 'Starch—composition, fine structure and architecture', *Journal of Cereal Science*, vol. 39, pp. 151–165, https://doi.org/10.1016/j.jcs.2003.12.001

Tian, L, Wang, M, Liu, Y, Su, Z, Niu, B, Zhang, Y, Dong, P & Long, D 2022, 'Multiple ionic conduction highways and good interfacial stability of ionic liquid-encapsulated cross-linked polymer electrolytes for lithium metal batteries', *Journal of Power Sources*, vol. 543, article 231848, https://doi.org/10.1016/j.jpowsour.2022.231848

UNEP 2022, *Emissions Gap Report 2022:* The Closing Window — Climate crisis calls for rapid transformation of societies, UNEP

Wang, J & Azam, W 2024, 'Natural resource scarcity, fossil fuel energy consumption, and total greenhouse gas emissions in top emitting countries', *Geoscience Frontiers*, vol. 15, article 101757, https://doi.org/10.1016/j.gsf.2023.101757

Wen, J, Zhao, Q, Jiang, X, Ji, G, Wang, R, Lu, G, Long, J, Hu, N & Xu, C 2021a, 'Graphene oxide enabled flexible PEO-based solid polymer electrolyte for all-solid-state lithium metal battery', *ACS Applied Energy Materials*, vol. 4, pp. 3660–3669, https://doi.org/10.1021/acsaem.1c00090

Wen, J, Zhao, Q, Jiang, X, Ji, G, Wang, R, Lu, G, Long, J, Hu, N & Xu, C 2021b, 'Graphene oxide enabled flexible PEO-based solid polymer electrolyte for all-solid-state lithium metal battery', *ACS Applied Energy Materials*, vol. 4, pp. 3660–3669, https://doi.org/10.1021/acsaem.1c00090

Whulanza, Y, Kusrini, E, Hermansyah, H, Sudibandriyo, M, Sahlan, M & Kartohardjono, S 2024, 'Catalyzing clean energy: the role of hydrogen and ammonia technology processes', *International Journal of Technology*, vol. 15, pp. 291–319, https://doi.org/10.14716/ijtech.v15i4.7171

Wijanarko, N, Wulandari, D, Arrafii, M, Ayu Pradanawati, S, Nimah, YL, Noerochim, L & Hamidah, N 2024, 'Effect of solid polymer electrolyte based on corn starch and lanthanum nitrate on the electrochemical performance of supercapacitor', *BIO Web of Conferences*, vol. 89, article 03001, https://doi.org/10.1051/bioconf/20248903001

Xia, L, Yu, L, Hu, D & Chen, GZ 2017, 'Electrolytes for electrochemical energy storage', *Materials Chemistry Frontiers*, vol. 1, pp. 584–618, https://doi.org/10.1039/C6QM00169F

Xu, X, Wang, B, Gao, W, Sui, J, Wang, J & Cui, B 2024, 'Effect of different proportions of glycerol and D-mannitol as plasticizer on the properties of extruded corn starch', *Frontiers in Nutrition*, vol. 10, https://doi.org/10.3389/fnut.2023.1335812

Yao, P, Yu, H, Ding, Z, Liu, Y, Lu, J, Lavorgna, M, Wu, J & Liu, X 2019, 'Review on polymer-based composite electrolytes for lithium batteries', *Frontiers in Chemistry*, vol. 7, p. 522, https://doi.org/10.3389/fchem.2019.00522

Zhong, C, Deng, Y, Hu, W, Qiao, J, Zhang, L & Zhang, J 2015, 'A review of electrolyte materials and compositions for electrochemical supercapacitors', *Chemical Society Reviews*, vol. 44, pp. 7484–7539, https://doi.org/10.1039/C5CS00303B